actuators

Article

Vibration Damping and Noise Reduction of a New Non-Newtonian Fluid Damper in a Washing Machine

Yuanjin Song [1,2], Zhong Zhuang [2,*], Xianping Wang [2], Qianfeng Fang [2], Zhijun Cheng [2] and Tao Zhang [3]

[1] Department of Materials Science and Engineering, University of Science and Technology of China, Hefei 230026, China; judysyj22@mail.ustc.edu.cn
[2] Institute of Solid State Physics, Chinese Academy of Sciences, Hefei 230031, China; xpwang@issp.ac.cn (X.W.); qffang@issp.ac.cn (Q.F.); zjcheng@issp.ac.cn (Z.C.)
[3] School of Physics and Materials Science, Guangzhou University, Guangzhou 510006, China; zhangtao@gzhu.edu.cn
* Correspondence: zzhuang@issp.ac.cn

Abstract: Due to friction vibration dampers' inability to effectively dampen low loads during high-frequency dewatering, drum washing machines vibrated intensively. In order to address this problem, in this paper, a novel type of low-cost non-Newtonian fluid damper is proposed and investigated based on the non-Newtonian fluid shear thinning properties' effect on vibration suppression during the high-frequency dewatering process of the washing machine. In contrast to other commonly used dampers, the homemade non-Newtonian fluid damper significantly suppresses the growth trend of the apparent elastic coefficient at high frequencies. A systematic investigation of damper structural parameters reveals that smaller gap height, higher piston head number, and more viscous fluid viscosity are adequate for vibration suppression and noise reduction. These results demonstrate that the non-Newtonian fluid damper can produce an excellent vibration-damping effect for the entire washing process of the washing machine, especially for the high-frequency dewatering process. The acceleration attenuation ratio can reach up to 83.49%, the energy attenuation is up to 98.44%, and the noise reduction is up to 10.38 dB.

Keywords: vibration damping; non-Newtonian fluid; noise reduction

Citation: Song, Y.; Zhuang, Z.; Wang, X.; Fang, Q.; Cheng, Z.; Zhang, T. Vibration Damping and Noise Reduction of a New Non-Newtonian Fluid Damper in a Washing Machine. *Actuators* **2024**, *13*, 9. https://doi.org/10.3390/act13010009

Academic Editors: Emiliano Pereira González and Sumeet S. Aphale

Received: 27 November 2023
Revised: 19 December 2023
Accepted: 21 December 2023
Published: 23 December 2023

1. Introduction

Home appliances are extensively used in people's ordinary lives, significantly lessening the domestic workload and raising their quality of life. The more comfortable experiences that people desire, the higher performance standards for household equipment need to be met. For instance, washing machines should operate quietly and smoothly in addition to washing clothing. However, the intensive mechanical vibration and dull noise of washing machines still need to be solved.

When a drum washing machine operates at high frequencies, the body vibrates severely, especially with only a small amount of clothing to dewater. The high-speed rotation of the eccentric system exacerbates system instability, while the existing vibration damping system, which consists of hanger springs and dampers (shown in Figure 1), fails to block the vibration transmission path effectively. Severe vibration not only interferes with the regular washing program but also wears down and damages the suspension system, shortening its lifespan. Solid-state friction dampers are widely employed in drum washers, accomplished by friction between the guide rod and ring. With the operating frequency increasing, the apparent elastic coefficient of the solid-state friction damper increases dramatically while the displacement decreases simultaneously. According to the amount of energy lost proportional to the relative moving distance between the two components, the vibration-damping performance is significantly reduced during dewatering.

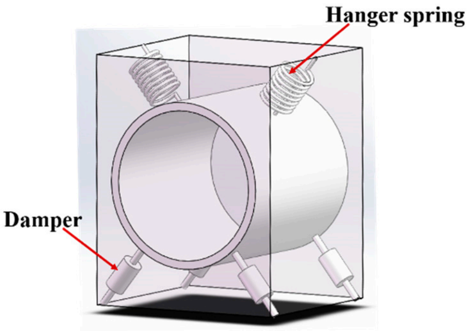

Figure 1. Drum washing machine and its vibration-damping system.

In order to reduce the vibration and noise of washing machines, researchers have been actively working on the development and implementation of magnetorheological dampers in recent years [1–4]. Spelta created a more effective semi-active magnetorheological (MR) damper to lower the machine's vibration and noise [5]. Phu designed a magnetorheological damper using a multi-coil construction and suggested an improved sliding mode control technique to manage washing machine vibration [6]. Nguyen modified the design of the magnetorheological damper configuration's design to minimize the washing machine's vibration caused by the imbalanced load [7]. Bui presented a self-supplied electromagnetic rheological damper that suppressed vibration by repurposing wasted energy [8]. Deng installed a semi-active, non-piston magnetic vibrator bar in a washing machine suspension system with lower damping forces and limitless working travel, halving the vibration acceleration [9]. Campos adopted the basic design of a ring-shaped power absorber to soak up vibration energy [10]. Liu utilized a controller to effectively lower the current pulsation rate of switching reluctance motors to decrease vibration and noise [11]. Buskiewicz created a brand-new electromechanical damper that separated throughout the rotating cycle to lessen frame vibration [12]. Min Gyu Jo utilized a robotic balancer to quicken the washing tank to reach steady-state vibration [13]. These damper structures have better damping performance than traditional friction dampers but also bring a few drawbacks. For magnetorheological vibration dampers, for instance, their internal structures are more complex, and the production cost is relatively high, which is unfavorable for mass production and wide application.

A non-Newtonian fluid damper is another type of vibration and shock damper commonly employed in vibration and shock situations, such as high-rise buildings, structural earthquakes, bridges, industrial pipe equipment earthquakes, ships, boats, etc. [14–19]. Given that the pseudoplastic fluid has the property of shear thinning (the shear stress increases slowly, and viscosity decreases rapidly with increasing frequency), as depicted by the red curve in Figure 2, it is anticipated that the pseudoplastic fluid damper will effectively overcome the shortcomings of inefficiency damping performance vibration in high-frequency friction dampers. The vibration impact force and amplitude of washing machines are much smaller than those of ships, buildings, and other large structures. Therefore, a novel kind of low to medium viscosity pseudoplastic non-Newtonian fluid damper is investigated in this work.

This paper systematically investigates the relationship between the chemical composition ratio of the damping fluid, the dimensional and structural parameters, the damper's mechanical strength, and damping performance. The results of the vibration experiments of the washing machine demonstrate that the new pseudoplastic fluid damper can effectively mitigate the vibration and noise of the machine, and the vibration suppression effect of low load eccentric operation is superior to the original solid-state friction damper. Moreover, the processing is simple, and the manufacturing cost is low, which would be beneficial to promote adoption and popularization.

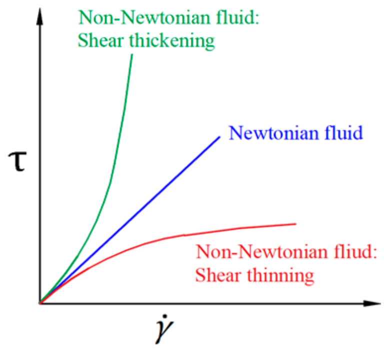

Figure 2. Shear stress-shear rate relationship for fluids.

2. Design and Theoretical Analysis of Non-Newtonian Fluid Damper

In order to optimize the damping effect of a washing machine damper under high-frequency operating circumstances, a non-Newtonian fluid damper is suggested to improve the damping force by adjusting the damping fluid ratio and the internal structural characteristics of the damper.

2.1. Design of Damper Damping Fluid

Carboxymethyl cellulose and xanthan gum are the primary components of the pseudoplastic fluid. Carboxymethyl cellulose (CMC) is an essential water-soluble cellulose ether [20]. Xanthan gum is an anionic extracellular polysaccharide extracted from Xanthomonas sp. [21]. Numerous hydrophilic groups, such as hydroxyl, acetyl, and pyruvic acid groups, are present in their molecules (Figure 3), and solid intermolecular hydrogen bonding significantly improves the viscosity and stability of the solution when dissolved in water [22–24]. Even at low concentrations of the polysaccharides, the CMC main chain has a significant amount of carboxymethyl groups [25], commonly used as cross-linking agents to create hydrogels. The xanthan gum chain structure undergoes an ordered-disordered transition from a helical to a coiled structure when dissolved at high temperatures, making it easier for the CMC side chains to cross-link. At the same time, CMC and XG also interact with each other, resulting in the high viscosity of the combined solution [26].

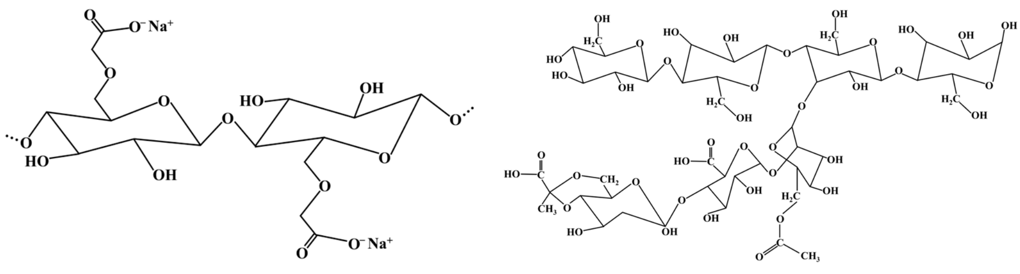

(**a**) (**b**)

Figure 3. Structural formulas of two polysaccharides: (**a**) carboxymethyl cellulose (CMC); (**b**) xanthan gum (XG).

Borax (B) and citric acid (CA) were added as crosslinking agents in order to increase their viscosity further [27]. B is an inorganic crosslinking agent widely employed in the creation of colloids, which crosslinks mixed CMC/XG solutions and dramatically increases the viscosity of the combined solution. B was hydrolyzed to form a boric acid/borate buffer solution, forming intermolecular hydrogen bonds with the hydroxyl groups in the XG structure [28]. B can be esterified with XG by heating, with at least three hydroxyl groups in the B molecule involved in forming the ester bond. At the same time, the dissolution of B results in a weakly alkaline solution, which also helps to raise crosslink density [29]. Furthermore, CA may create intermolecular covalent diester connections with CMC and

XG polysaccharides [30]. The cross-linking causes the polymers' molecular chains to grow more significantly, enhancing the combined solution's viscosity.

2.2. Mechanical Model of the Gap Fluid Damper

Typical viscous dampers typically have a cylindrical construction. Depending on the different energy-consuming components, it can be classified as an orifice, gap, or mixed viscous damper [31]. The gap viscous damper has the most straightforward construction, low manufacturing requirements, and assembly precision. As shown in Figure 4, there is a gap between the piston head's side and the cylinder's inner wall. When an external force drives the piston head of the damper to perform the reciprocating motion, the variation in pressure between the two ends of the damping head causes fluid to flow from one side to the other through the gap. The experimentally designed non-Newtonian fluid damper has a gap viscous damper-like structure.

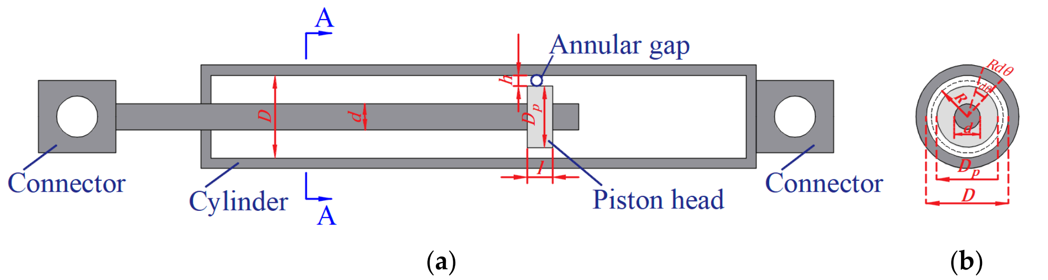

Figure 4. Internal configuration of annular gap-type viscous damper: (**a**) damper with an annular gap; (**b**) A-A section view.

Considering the rheological characteristics of the non-Newtonian fluid, the force on the fluid can be analyzed based on the Navier–Stokes empirical equations. As shown in Figure 5, the fluid unit in the gap is subjected to shear force, pressure, and inertia force. According to the force equilibrium condition of the fluid unit, it can be expressed as

$$\rho \frac{\partial v}{\partial t} = \frac{\partial \tau}{\partial y} - \frac{\partial p}{\partial x} \tag{1}$$

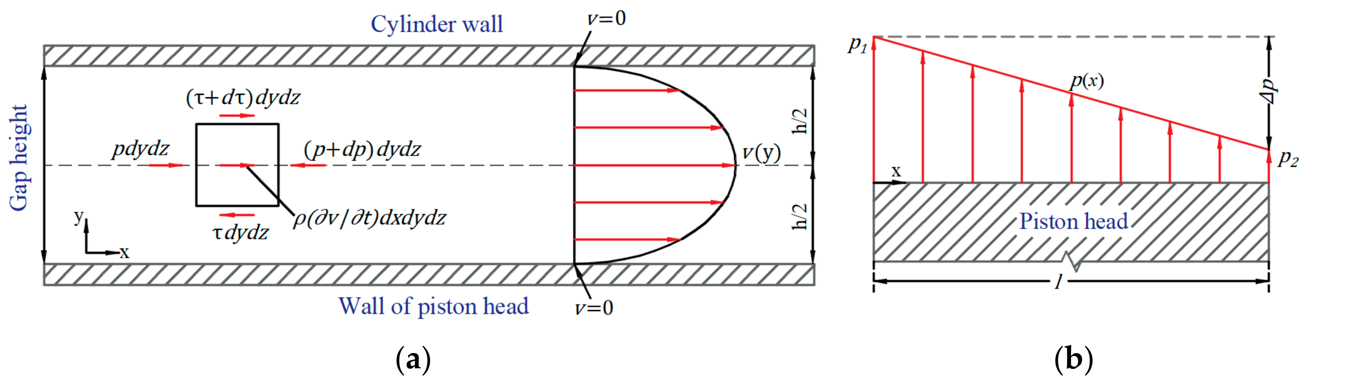

Figure 5. Fluid state in the gap: (**a**) unit fluid element and flow velocity profile; (**b**) pressure difference.

v is the flow velocity of the fluid cell, and therefore $\rho(\partial v/\partial t)$ is the inertial force per unit volume of fluid; τ is the shear force acting on the surface of the fluid cell; p is the internal pressure; $\partial p/\partial x$ is the pressure gradient, which can be written as a constant $\Delta p/l$ (Δp is the pressure difference between the two sides of the piston head, as shown in Figure 5b, and l is the thickness of the piston head) for an incompressible fluid.

It can be assumed that only laminar flow is produced because the composite fluid used in the experiment is homogeneous, and there is no exchange of volume elements between the layers. Since the fluid's viscous force is substantial and the inertial force is negligible in comparison, Equation (1) can be abbreviated as follows:

$$\frac{\partial \tau}{\partial y} = \frac{\Delta p}{l}. \tag{2}$$

Integrating both sides of Equation (2)

$$\tau(y) = \frac{\Delta p}{l} y. \tag{3}$$

The composite fluid medium used in the experiment is a non-Newtonian fluid with a specific viscosity that exhibits shear-thinning properties (Figure 2). Its shear stress and shear rate can be stated as follows [32]:

$$\tau(y) = k[\dot{\gamma}(y)]^{\alpha} \tag{4}$$

where k is the fluid viscosity coefficient, α is the velocity index, for shear-thinning type fluid $\alpha < 1$, $\tau(y) = \partial v / \partial y$, as shown in Figure 5a, combining Equation (4):

$$\frac{\partial v}{\partial y} = \left(\frac{\tau(y)}{k}\right)^{\frac{1}{\alpha}}. \tag{5}$$

As shown in Figure 4, D is the cylinder bore diameter, Dp is the diameter of the piston head, d is the actuator diameter, h is the gap height, and is the radius of the center ring of the gap. The flow rate of fluid dQ was calculated within the range of $d\theta$. The viscous fluid flows in a circular tube in a laminar manner, and the velocity distribution is a rotating paraboloid. Therefore, the boundary conditions are introduced as follows:
when $y = \frac{h}{2}$, $v(y) = 0$
when $y = -\frac{h}{2}$, $v(y) = 0$

The equation for dQ can be obtained combining Equation (5):

$$dQ = \int_{-\frac{h}{2}}^{\frac{h}{2}} v(y) R d\theta dy = -2R d\theta \int_{0}^{\frac{h}{2}} y \left(\frac{\Delta p}{lk} y\right)^{\frac{1}{\alpha}} dy. \tag{6}$$

The total flow equation is obtained as follows:

$$Q = \frac{\pi (D + Dp) \alpha h^{\frac{2\alpha+1}{\alpha}}}{4(2\alpha + 1)} \left(\frac{\Delta p}{2lk}\right)^{\frac{1}{\alpha}}. \tag{7}$$

The pressure difference between the two sides of the piston head can be obtained from Equation (7):

$$\Delta p = \frac{2lkQ^{\alpha}}{h^{2\alpha+1}} \left[\frac{4(2\alpha + 1)}{\pi (D + Dp) \alpha}\right]^{\alpha} \tag{8}$$

$$Q = SVp \tag{9}$$

where, S is the practical action area of the piston head, $S = \pi (Dp^2 - d^2)/4$, Vp is the motion speed of the piston head.

Substituting Equation (9) into Equation (8), the damping force can be expressed as:

$$F = \Delta p S = \frac{\pi l k (Dp^2 - d^2)}{2h^{2\alpha+1}} \left[\frac{(2\alpha + 1)(Dp^2 - d^2)}{(D + Dp)\alpha}\right] (Vp)^{\alpha}. \tag{10}$$

2.3. Design of Non-Newtonian Fluid Damper Structure

Analyzing Equation (10), it can be seen that two main factors influence the size of the output damping force of the gap fluid damper: one is the internal structural parameters, such as the inner diameter of the damper cylinder and the height of the gap, and the other is the parameters related to the fluid's viscosity. In order to make comparisons with the friction damper easier, the piston rod length, cylinder length, outer diameter, and inner diameter of the non-Newtonian fluid damper are kept the same size as the friction type. When the structural characteristics of the damper are examined, changing the diameter of the piston head, increasing the number of piston heads, and altering the viscosity of the non-Newtonian fluid are significant ways to achieve the modification of the damping force. By methodically examining the impact of these three factors on the output damping force and vibration suppression capacity of the damper, the optimum vibration suppression process parameters are designed to provide high-performance washing machine vibration damping.

3. Performance Tests of Non-Newtonian Fluid Dampers

3.1. Formulation of Damping Fluids for Non-Newtonian Fluids

Carboxymethyl cellulose (CMC) and citric acid (CA) were purchased from Aladdin Reagent (Shanghai, China), food grade; Xanthan gum (XG) was purchased from Ceratonia SA (Murcia, Spain), food grade; borax ($Na_2B_4O_7{\cdot}10H_2O$) was purchased from Beichen Founder Reagent (Tianjin, China), analytically pure; ethylene glycol was purchased from Shanghai Titan (Shanghai, China), analytically pure; and the water used for experiments was ultrapure water prepared with Dow Ultra Pure Water System (TS-D1-10L/H).

A specific mass of CMC powder was dissolved in water while stirring at 60 °C to obtain CMC mother liquor. A specific mass of XG powder was taken, and the above operation was repeated to obtain XG mother liquor. A series of CMC/XG mixed solutions were prepared by mixing the CMC mother liquor and the XG mother liquor, in which the mass concentrations ρ(p) of polysaccharides (CMC + XG) were 1.5 g/L, 2.0 g/L, 3.0 g/L, and 4.0 g/L, respectively. The right amount of the combined solution was taken, borax, citric acid, and ethylene glycol were added, and everything was well mixed to create the non-Newtonian fluid known as the CMC/XG/B/CA crosslinked solution. The mass fraction of composition and the mass concentration of each solute are listed in Table 1.

Table 1. Composition of damping fluid.

Mass Fraction ω (%)		**Mass Concentration ρ (g/L)**		
CMC	**XG**	**B**	**CA**	**EG**
30	70	1.5	2.0	2.5

The formulated solutions were held at room temperature for 24 h, and then the room temperature (25 °C) viscosity was tested using a rotating rheometer (DHR2) from TA Instruments, New Castle, DE, USA.

3.2. Design of Damper Specimens

The non-Newtonian fluid variable damping damper is depicted schematically in Figure 6 as a single-cavity construction with the piston head, the fluid cylinder, the sealing ring, the piston rod, and the connector. The damper's principal structural dimensions are listed in Table 2.

Table 2. Main structural dimensions of the damper (all dimensions in mm).

Dimension	**Connector**	**Piston Rod**	**Cylinder**
Length	25	50	110
Diameter	20	10	20

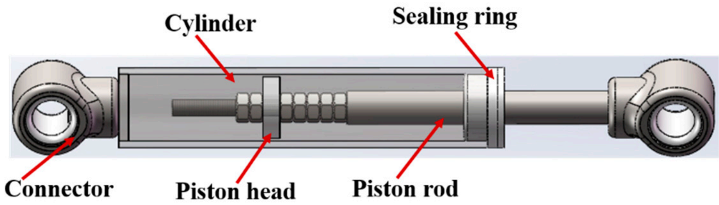

Figure 6. Structure of non-Newtonian fluid variable damping damper.

One end of the cylinder is closed, and the other is open and encapsulated by a sealing ring to form a vibration-damping sealing chamber inside the cylinder. The piston rod is attached to the piston head and extended into the vibration-damping chamber. A prepared non-Newtonian fluid solution filled the sealing chamber with a volume ratio of around 75%. When the piston rod is driven by an external force for reciprocating motion, the fluid flows in the fluid cylinder under the impetus of the piston head, generating a damping force. The diameter of the damping head Dp, the number of damping heads n, and the viscosity of the damping fluid are the three factors considered for the damper specimens. The piston rod and cylinder inner diameters remain constant, while the other structural dimensions change as variables.

3.3. Mechanical Properties Testing of Dampers

The mechanical properties of the damper were tested using the Shimadzu EHF-E electro-hydraulic servo fatigue testing machine, as shown in Figure 7. When the washing machine's vibration frequency was examined, it was found that the usual washing frequency was around 6 Hz, and the average spinning frequency was approximately 10–13 Hz. Based on this frequency range, the mechanical properties of the original solid-state friction damper and fluid damper (damping head diameter of 18.4 mm, number of damping heads of 4, and damping fluid ρ(p) = 2.0 g/L) were tested at frequencies of 1 Hz, 5 Hz, and 10 Hz, with a displacement amplitude of ±5 mm, at room temperature of 20 °C.

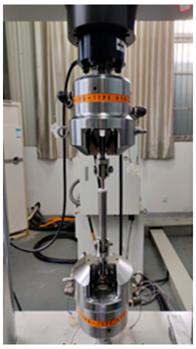

Figure 7. Test of mechanical properties of damper.

3.4. Damping Performance and Noise Testing

The washing machine for this experiment is a Swan drum washer (TD100VT096WDG) manufactured by Midea (Foshan, China), with a washing load of 10 kg. The suspended drum is connected to the top of the casing by two hanger springs above it, and the bottom of the suspended drum is connected to the bottom of the casing by four vibration dampers. The drum has a maximum speed of 1400 rpm and may rotate clockwise and counterclockwise. The drum only moves in a circular motion while spinning under balanced load circumstances [33]. An uneven load causes certain lateral and vertical motions of the inner cylinder to be transmitted to the outer surface of the machine through the action of springs and dampers, which is the primary cause of vibration.

In order to analyze the vibration of the washing machine during a period of complete working conditions, each experiment was carried out using the fast wash mode of the machine system for a duration of approximately 1050 s, which included three washing periods (90~220 s, 360~450 s, and 620~710 s) and one dewatering period (910~1050 s). An eccentric mass metal block of 300 g is attached to the inner wall of the test drum by magnets for low-load vibration-damping performance tests.

The vibration acceleration signals were measured by a Dytran 3313 Triaxial Acceleration Sensor (Chatsworth, CA, USA) and a DH8303 Dynamic Signal Test and Analysis System with a sampling frequency of 1 kHz. Two triaxial acceleration sensors were mounted on the washing machine's outside drum wall and the bottom of the machine body, respectively, to compare the damping curves before and after the vibration passes through the damper, as shown in Figure 8. In this experiment, the x-axis, y-axis, and z-axis denote the horizontal, lateral, and vertical direction, respectively.

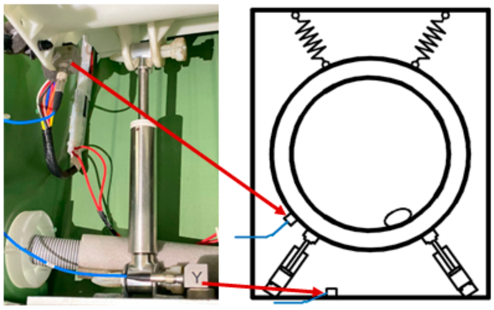

Figure 8. Damper and acceleration sensor mounting location.

Instantaneous noise levels under machine operating conditions were collected using an AR844 Noise Meter, and the average sound pressure level values of the noise using fluid dampers and solid-state friction dampers were calculated. Referring to GB-T4288-2003 "Domestic Electric Washing Machine", the test was carried out in a semi-anechoic chamber, as shown in Figure 9; the numbers 1~4 are the placement positions of the noise meter microphone, with the center point at the bottom of the washing machine as the origin (0, 0, 0), according to the outer dimensions of the washing machine, the coordinates of the four points from 1 to 4 are calculated as (0, 1.2975, 0.925), (−1.265, 0, 0, 0.925), (0, −1.2975, 0, 0.925) and (1.265, 0, 0.925), respectively. 0.925), (0, −1.2975, 0.925) and (1.265, 0, 0.925) (All dimensions in mm).

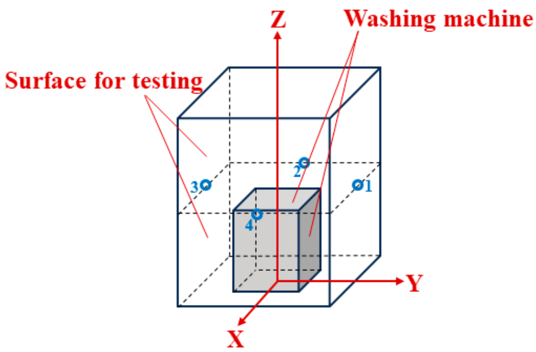

Figure 9. Noise meter microphone position.

4. Performance Test Results and Discussion

4.1. Rheological Property

The rheological curves of the CMC/XG/B/CA crosslinked solutions were determined, where ρ(p) was 1.5 g/L, 2.0 g/L, 3.0 g/L, and 4.0 g/L. The apparent viscosity of the composite solutions rapidly drops with an increase in shear rate, as seen from the measured data in Table 3, clearly demonstrating shear-thinning features. The drum washing machine used in this experiment has a rotational speed of about 200–1400 rpm under working conditions, which is converted to a shear rate of about 2–18 s^{-1}.

Table 3. Data of apparent viscosity variation with shear rate (the unit of viscosity is Pa·s).

Shear Rate (s^{-1})	ρ(p) = 1.5 g/L	ρ(p) = 2.0 g/L	ρ(p) = 3.0 g/L	ρ(p) = 4.0 g/L
0.12	2.79	18.16	29.38	42.50
0.18	2.73	17.02	27.51	40.24
0.28	2.63	16.03	23.75	33.33
0.42	2.37	14.69	18.83	24.44
0.67	2.11	12.28	15.31	17.87
1.05	1.59	8.55	11.63	14.56
2.55	1.49	4.83	6.85	9.81
3.99	1.25	3.43	4.80	7.46
6.23	0.92	2.58	4.00	5.71
9.73	0.06	1.43	3.00	4.70
15.22	0.52	1.14	2.19	3.81

According to Figure 10, the apparent viscosity rapidly drops in the shear rate range of 1–16 s^{-1}. Figure 11 shows the frequency domain signal of the vibration signal of the washing machine collected by the acceleration sensor. The FFT analysis shows that the regular washing frequency of the washing machine is about 6 Hz, and the dewatering frequency is about 10–13 Hz. This working frequency range corresponds to the shear-thinning rate range of the solution in Figure 10. When the rotational speed of the washing machine is gradually accelerated, the piston head of the damper accelerates under the action of the external force. The viscosity of the damping fluid in contact with it decreases so that the damping force of the damper with this damping fluid in the high-frequency operating conditions of the washing machine is significantly reduced relative to that of the low-frequency output damping force.

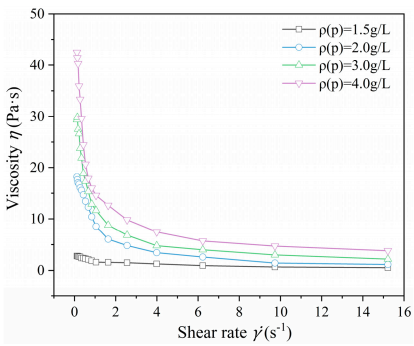

Figure 10. Rheology curves of CMC/XG/B/CA solutions.

4.2. Apparent Elastic Coefficient of the Damper

The output force-displacement relationship of the non-Newtonian fluid damper and the solid-state friction damper can be acquired by the fatigue testing machine, and the apparent elastic coefficient of the damper can be defined by the ratio of the maximum values of the force and displacement. Figure 12 displays the two types of dampers' apparent elastic coefficients about the test frequency. Under constant amplitude ± 5 mm, the solid-state friction damper has a stiffer structure than the non-Newtonian fluid damper because of its higher output force. The stiffness of solid-state friction dampers rises considerably as frequency increases, whereas non-Newtonian fluid dampers barely change with frequency. Therefore, non-Newtonian fluid dampers can effectively overcome the defects of solid-state friction dampers at high frequencies due to the decrease in viscosity.

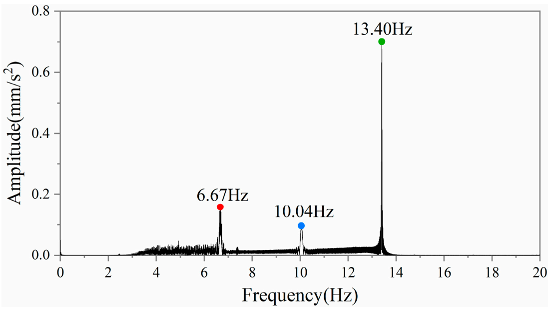

Figure 11. FFT Analysis of vibration frequency.

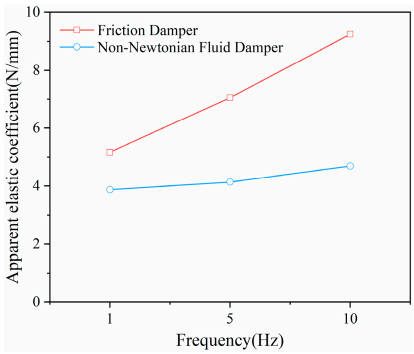

Figure 12. Variation of apparent elastic coefficient of dampers with frequency.

4.3. Vibration Suppression Effect

The vibration damping experiments were conducted to test the vibration in a drum washing machine. First, the fluid damper equipped with various damping fluids is tested. Then, the damper structure parameters are changed following the variables affecting the damping force calculated in the previous section. The solid-state friction damper is also tested for comparison. Three variables were considered for the damper test specimens: the diameter of the damping head, the number of damping heads, and the fluid's viscosity. Due to the large number of specimen types, the following description rule is used to differentiate between the specimens: taking SP-1-*n*4-F_2 as an example, 1 and 2 indicate the piston head diameters of 18.4 mm and 18.8 mm, respectively; *n*1–*n*4 represent the number of piston heads from 1 to 4; F_w and F_p represent the damping fluid as water and Polydimethylsiloxane, and F_1, F_2, F_3, and F_4 represent the damping fluids of ρ(p) = 1.5 g/L, ρ(p) = 2.0 g/L, ρ(p) = 3.0 g/L, and ρ(p) = 4.0 g/L, respectively. In the following, the effects of different kinds of damping fluids on the damping effect will be investigated to analyze the effectiveness of non-Newtonian fluids for vibration suppression. Then, according to the variables, three subsections will be addressed to discuss the effects of these three variables on the control of vibration and noise of the washing machine for better damping performance.

4.3.1. Effect of the Type of Damping Fluid

The diameter of the damping head was found to be 18.8 mm based on the size of the inner diameter of the damper cylinder. In order to examine the effects of various damping forces, four damping heads were assembled and fixed at the end of the actuator. Based on damper rod length and fluid chamber depth, the interval distance of the damping heads was 8 mm, and the thickness of the damping heads was 5 mm.

In order to investigate the efficacy of self-formulated non-Newtonian fluids on vibration damping, water, Polydimethylsiloxane, and CMC/XG/B/CA solutions were used as damping fluids. Polydimethylsiloxane is a commonly used damping oil for viscous fluid dampers, with the chemical formula $(C_2H_6OSi)_n$. To ensure similar viscosity of non-

Newtonian fluids, the damping fluid was chosen to be ρ(p) = 3.0 g/L, and the viscosity of Polydimethylsiloxane was chosen to be 12,500 cst (static state). A second set of dampers without damping fluid and a set of dampers with water were set up for evidence of whether the non-Newtonian fluid could optimize the damping effect. The dimensions and design parameters of the designed dampers are listed in Table 4.

Table 4. Specimen characters (dimensions in mm, *n* is number of piston heads, *l* is thickness of piston head, *Dp* is diameter of piston head, *d* is diameter of piston rod, *h* is height of gap).

Specimen	*n*	*l*	*Dp*	*d*	*h*	Fluid
SP-2-*n*4-F_3	4	5	18.8	10	0.6	ρ(p) = 3.0 g/L
SP-2-*n*4-F_0	4	5	18.8	10	0.6	None
SP-2-*n*4-F_p	4	5	18.8	10	0.6	$(C_2H_6OSi)_n$
SP-2-*n*4-F_w	4	5	18.8	10	0.6	Water

Because the acceleration sensor fixed on the wall of the damper cylinder is rigidly connected to the vibration source, the accelerometer at this place measures the vibration acceleration of the drum. In Figure 13, the solid-state friction damper in the dewatering stage and the vibration acceleration of the four specimens in Table 4 are compared at typical speeds of 400–1200 rpm, corresponding to high-frequency operating circumstances. Figure 13a presents the vibration acceleration obtained from the top triaxial accelerometer measured in the z (vertical) direction, and Figure 13b shows the vibration acceleration on the bottom panel of the washing machine where the other end of the damper is fixed. According to the figure, when there is 300 g of eccentricity, the top vibration acceleration in the z-direction of the four specimens is almost equal to that of the solid friction damper. However, the bottom vibration acceleration is much less than that of the solid friction damper. It is shown that the reduction of the apparent elastic coefficient of the non-Newtonian fluid damper results in a vibration suppression effect. The vibration acceleration at the bottom of the damper using a homemade non-Newtonian fluid (SP-2-*n*4-F_3) was further reduced compared to the specimen with none fluid (SP-2-*n*4-F_0), water (SP-2-*n*4-F_w), and Polydimethylsiloxane (SP-2-*n*4-F_p). The suppression of bottom vibration employing specimen SP-2-*n*4-F_3 is more effective, and the bottom acceleration amplitude is 47.27% lower compared to the solid-state friction damper.

The spinning program can be divided into three stages according to the magnitude of the vibration, corresponding to the three speeds of the washing machine under high-frequency conditions, i.e., 400 rpm, 800 rpm, and 1200 rpm. In order to facilitate the comparison, we took the average acceleration values of three-speed stages in a fixed period for Figure 14. Compared to the solid-state friction type, the fluid damper specimen exhibits a lower vibration acceleration value. The average bottom vibration acceleration value in the z-direction with SP-2-*n*4-F_3 is substantially the smallest among the other four fluid damper specimens, and the average acceleration value of the three rotational speed phases is lower by 72.61%, 84.30%, and 81.80%, respectively. The corresponding vibration energy was attenuated by 92.49%, 97.53%, and 96.69%, respectively.

It is necessary to normalize the acceleration peaks measured at the wall (top) and bottom of the washing machine to compare the acceleration decay degree of the fluid damper specimens with that of a solid-state friction damper under the same external circumstances [34]. The acceleration attenuation ratio is defined as:

$$i = \frac{Apb}{Apt} \tag{11}$$

where, Apt is the peak acceleration recorded by the top accelerometer, Apb is the peak acceleration measured along the bottom centerline.

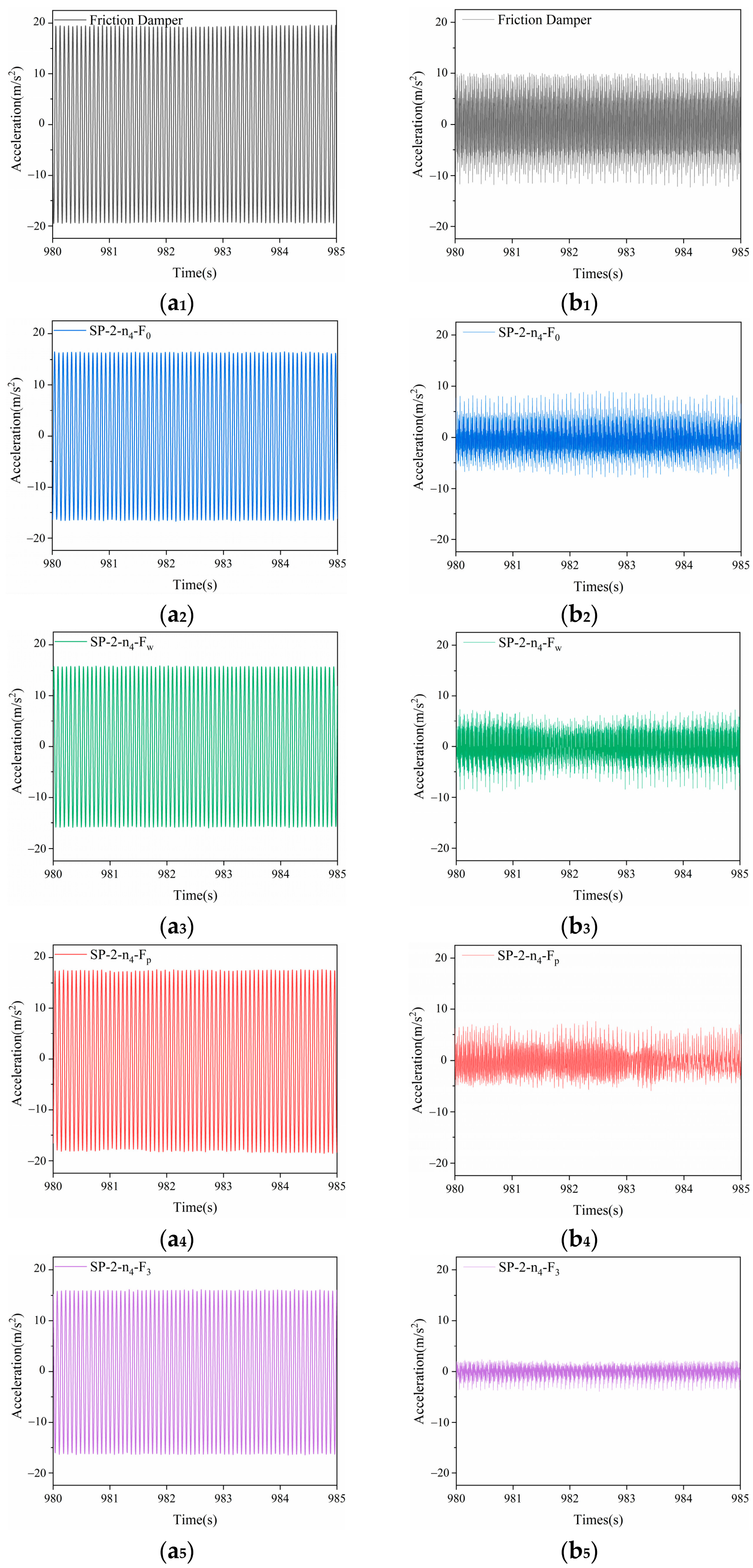

Figure 13. Acceleration of the dewatering stage: ($\mathbf{a_1}$–$\mathbf{a_5}$) Top acceleration in the z-direction; ($\mathbf{b_1}$–$\mathbf{b_5}$) Bottom acceleration in the z-direction.

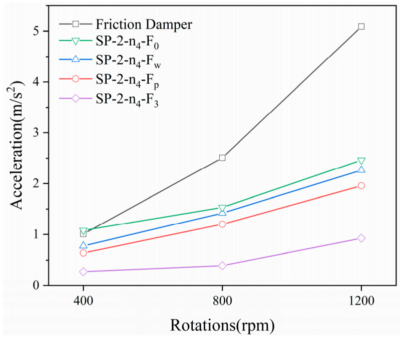

Figure 14. Bottom acceleration in the z-direction for three speed stages.

Figure 15 shows the acceleration attenuation ratio curves for the fluid and friction damper specimens at three speed stages. The smaller the *i* value is, the smaller the vibration energy transferred from the top to the bottom under the same rotational speed condition when the top acceleration values are similar. As can be seen, the specimen with the fluid damper has a decreased *i* at speeds higher than 400 rpm, demonstrating that the self-designed fluid damper can enhance the damping system of the washing machine's capability to suppress vibration. And the *i* of specimen SP-2-*n*4-F_3 was found to perform significantly better when compared to the solid-state friction type. This suggests that employing the formulated non-Newtonian fluid as the fluid damper filler fluid may further increase the vibration suppression effect. Out of all specimens, fluid damper specimen SP-2-*n*4-F_3 exhibits superior vibration suppression properties in the system; the acceleration attenuation ratios at 400, 800, and 1200 rpm decreased by 57.55%, 69.28%, and 72.11% in comparison to the solid-state friction damper's values.

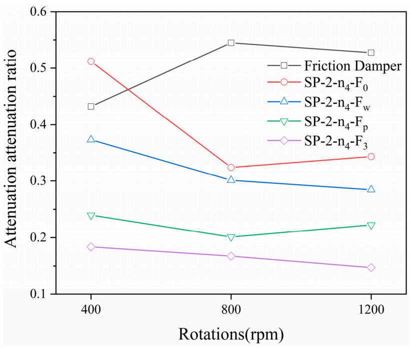

Figure 15. Acceleration attenuation ratio.

Figure 16 displays the vibration acceleration of the solid-state friction damper and SP-2-*n*4-F_3 during the washing stage at around 200 rpm, which corresponds to low-frequency circumstances. Figure 16a shows the vibration acceleration measured by the triaxial accelerometer on the bottom panel in the z (vertical) direction, and Figure 16b shows the vibration acceleration in the y (lateral) direction. The x (horizontal) direction is not shown because the vibration is slight. From both figures, it can be seen that specimen SP-2-*n*4-F_3 performs better during the washing stage, the bottom vibration acceleration in the z and y directions is smaller than that of the friction damper, and the amplitude fluctuation is smoother, indicating that its energy-consuming ability is more potent than that of friction damper under this rotational speed.

4.3.2. Influence of Piston Head Diameter (Dp)

Based on the damper cylinder's inner diameter, two damping head sizes, 18.4 mm and 18.8 mm, were chosen for comparison experiments. The number of piston heads was 4, and the spacing and thickness remained the same as in the previous experiments. The geometrical dimensions and design parameters of the two designed dampers are listed in Table 5.

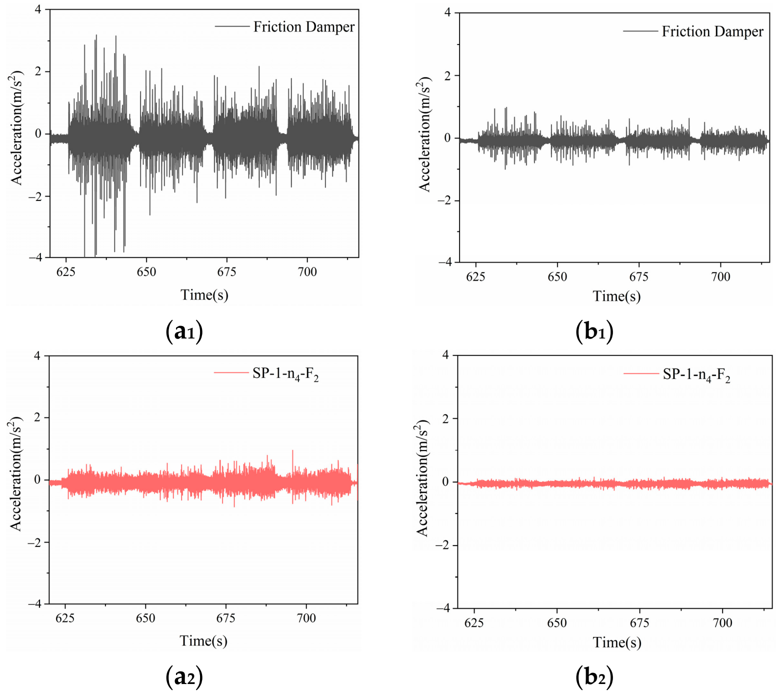

Figure 16. Acceleration of the washing stage (friction damper and specimen SP-2-*n*4-F_3): (**a_1**,**a_2**) bottom acceleration in the z-direction; (**b_1**,**b_2**) bottom acceleration in the y-direction.

Table 5. Specimen characters (dimensions in mm, *n* is number of piston heads, *l* is thickness of piston head, *Dp* is diameter of piston head, *d* is diameter of piston rod, *h* is height of gap).

Specimen	*n*	*l*	*Dp*	*d*	*h*	Fluid
SP-1-*n*4-F_2	4	5	18.4	10	0.8	ρ(p) = 2.0 g/L
SP-2-*n*4-F_2	4	5	18.8	10	0.6	ρ(p) = 2.0 g/L

Figure 17 shows the comparison of vibration acceleration of SP-1-*n*4-F_2 and SP-2-*n*4-F_2 in the dewatering stage. The vibration acceleration values at the top of the z-direction for specimens SP-1-*n*4-F_2 and SP-2-*n*4-F_2 are shown in the figure to be reasonably close to each other. However, the vibration amplitude at the bottom of SP-1-*n*4-F_2 is reduced by more than 50% when compared to the Figure 13a solid-state friction type. When the diameter of the damping head increases from 18.4 mm to 18.8 mm, i.e., the height of the gap decreases, the damping force increases, and the acceleration further decreases, the acceleration amplitude at the bottom of the specimen SP-2-*n*4-F_2 is only equivalent to 35% of that of the solid-state friction type.

Figure 18 clearly shows that the bottom vibration acceleration of specimens SP-1-*n*4-F_2 and SP-2-*n*4-F_2 in the z and y directions is significantly smaller than that of the solid-state friction damper, acceleration value attenuation is mostly more than 62.70%, the highest reaches 84.30%. When the rotational speed is above 800 rpm, the corresponding vibration energy attenuation is more than 90%. Furthermore, it is discovered that specimen SP-2-*n*4-F_2 has a lower acceleration amplitude in the z and y directions than specimen SP-1-*n*4-F_2, with the z direction showing a more evident drop. This reduces the average acceleration of the three rotational speed phases of 39.61%, 17.00%, and 40.02%, respectively. It suggests that a slight increase in the diameter of the piston head, i.e., a reduction in the gap height, can lead to a better energy dissipation capacity and enhance the damping performance of the designed fluid damper. Comparing Figures 16–18 demonstrates that the fluid dampers designed for this study consume more vibration energy at both low and high spinning frequencies than the commonly used solid-state friction damper.

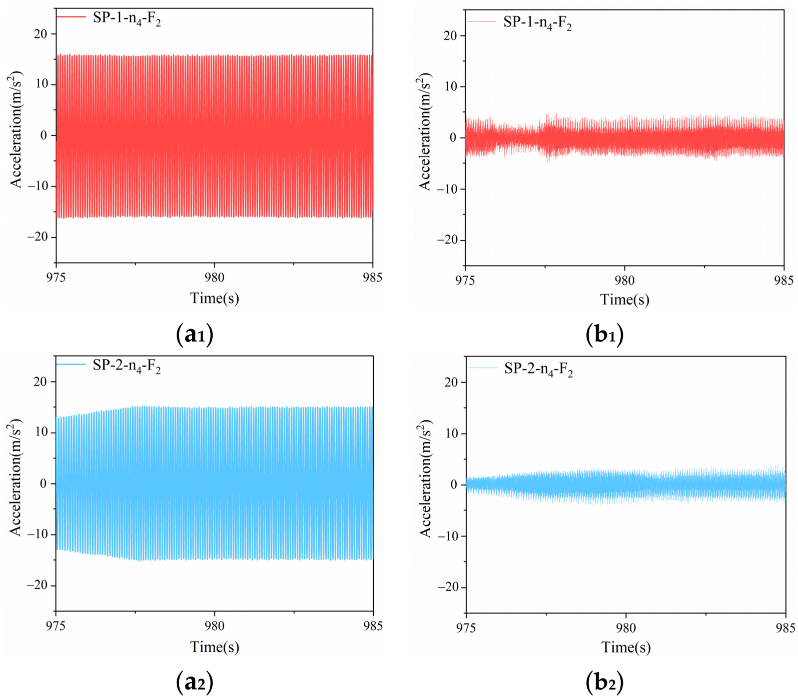

Figure 17. Acceleration of the dewatering stage (friction damper and specimen SP-1-*n*4-F_2, SP-2-*n*4-F_2): (**a_1**,**a_2**) top acceleration in the z-direction; (**b_1**,**b_2**) bottom acceleration in the z-direction.

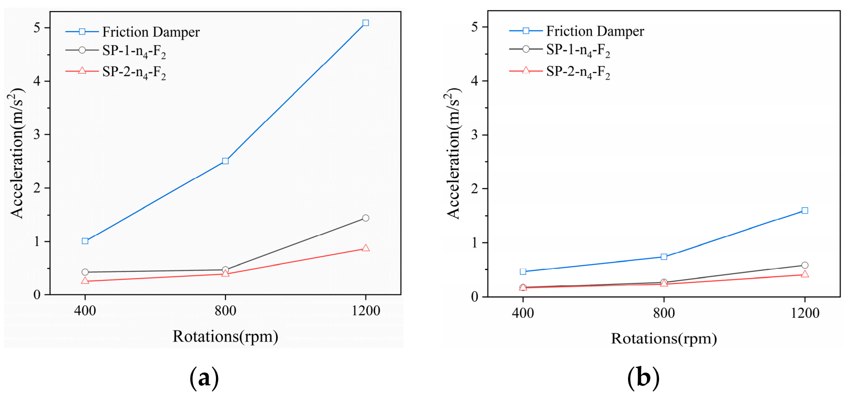

Figure 18. Average acceleration for three speed stages (SP-1-*n*4-F_2 and SP-2-*n*4-F_2): (**a**) bottom acceleration in the z-direction; (**b**) bottom acceleration in the y-direction.

4.3.3. Influence of Fluid Viscosity

The geometries and the design parameters of the eight damper types designed for fluid viscosity are listed in Table 6. Figure 19 indicates the vibration acceleration in the z and y directions at the bottom throughout the dewatering stage. It is easy to conclude that when the diameter of the damping head is 18.4 mm, the acceleration amplitude of specimen SP-1-*n*4-F_4 in the z and y directions is the smallest compared to the other three during the entire dewatering process. Increasing the viscosity of the damping fluid can enhance the vibration suppression effect of the fluid damper. According to Figure 20, in comparison with SP-1-*n*4-F_1, the average vibration acceleration of SP-1-*n*4-F_4 reduces by 70.01%, 67.39%, and 55.67% for the three rotational speed stages in both directions, respectively. This finding further demonstrates that enhancing the viscosity of the damping fluid can improve the fluid damper's ability to suppress vibration.

Table 6. Specimen characters (dimensions in mm, *n* is number of piston heads, *l* is thickness of piston head, *Dp* is diameter of piston head, *d* is diameter of piston rod, *h* is height of gap).

Specimen	*n*	*l*	*Dp*	*d*	*h*	Fluid
SP-1-n4-F_1	4	5	18.4	10	0.8	ρ(p) = 1.5 g/L
SP-1-n4-F_2	4	5	18.4	10	0.8	ρ(p) = 2.0 g/L
SP-1-n4-F_3	4	5	18.4	10	0.8	ρ(p) = 3.0 g/L
SP-1-n4-F_4	4	5	18.4	10	0.8	ρ(p) = 4.0 g/L
SP-2-n4-F_1	4	5	18.8	10	0.6	ρ(p) = 1.5 g/L
SP-2-n4-F_2	4	5	18.8	10	0.6	ρ(p) = 2.0 g/L
SP-2-n4-F_3	4	5	18.8	10	0.6	ρ(p) = 3.0 g/L
SP-2-n4-F_4	4	5	18.8	10	0.6	ρ(p) = 4.0 g/L

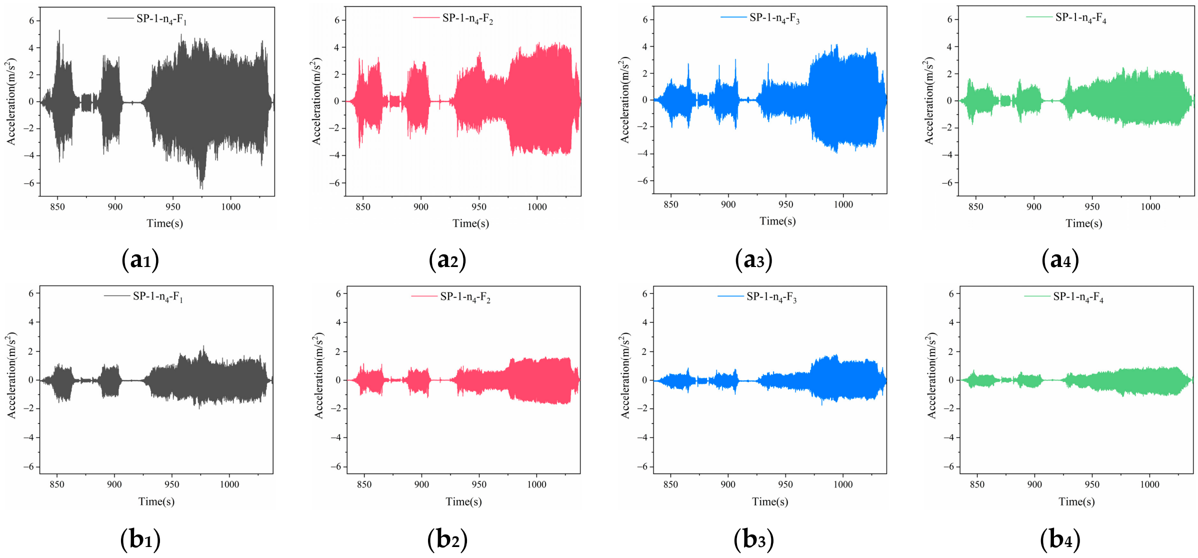

Figure 19. Acceleration of the dewatering stage (the diameter of the piston head of the specimen is 18.4 mm and the number of piston heads is 4, changing the damping liquid): (**a_1**–**a_4**) bottom acceleration in the z-direction; (**b_1**–**b_4**) bottom acceleration in the y-direction.

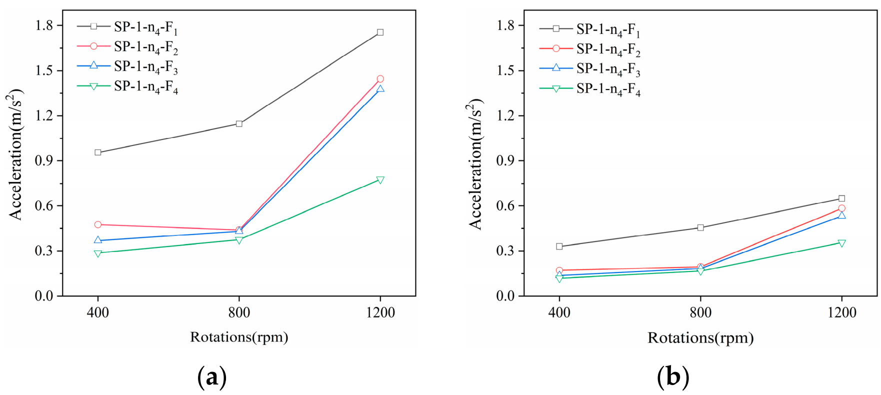

Figure 20. Average acceleration for three speed stages (the diameter of the piston head of the specimen is 18.4 mm and the number of piston heads is 4, changing the damping liquid): (**a**) bottom acceleration in the z-direction; (**b**) bottom acceleration in the y-direction.

When the diameter of the damping head increases to 18.8 mm (Figure 21), the average acceleration values of the three-speed phases of dewatering are compared. Compared with the other specimens, the acceleration in the z and y directions of specimen SP-2-n4-F_3 is lower, and the vibration-damping effect is better. However, the increase in viscosity at this time led to the continual reduction of vibration. An increase in the piston head diameter or piston head number cannot always enhance the effects of vibration suppression, suggesting that there is not a straightforward linear relationship between the two variables.

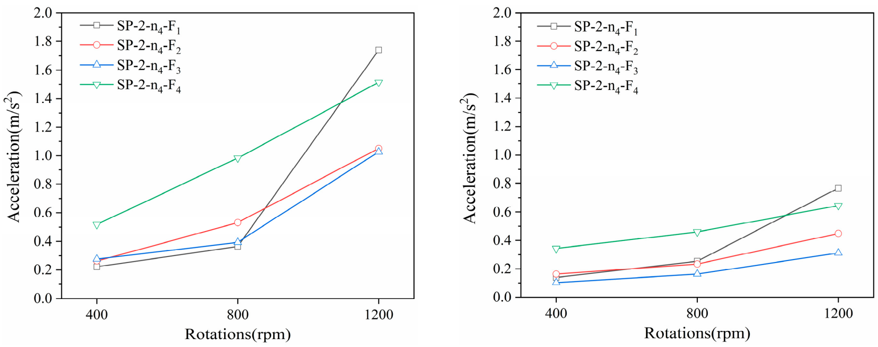

(**a**) (**b**)

Figure 21. Average acceleration for three speed stages (The diameter of the piston head of the specimen is 18.8 mm and the number of piston heads is 4, changing the damping liquid): (**a**) bottom acceleration in the z-direction; (**b**) bottom acceleration in y-direction.

4.3.4. Influence of the Number of Piston Heads (n)

The geometries and design parameters of the 12 damper types designed for fluid viscosity are listed in Table 7. It was discovered that the accelerations of specimens SP-2-n3-F_2, SP-2-n2-F_3, and SP-2-n1-F_4 in the z-direction are lower when compared to the average acceleration values of the dewatering stage in Figure 22. Additionally, the average acceleration of the three rotational speed phases is reduced by 51.82%, 87.51%, and 87.33%, respectively, and the corresponding energy is attenuated by 76.79%, 98.44%, and 98.39% compared to that of the solid-state friction damper, which indicates that it has the most apparent suppression effect on the system's vibration. Among these three specimens, the SP-2-n1-F_4 specimen has the smallest acceleration value in the z-direction.

Table 7. Specimen characters (dimensions in mm, n is number of piston heads, l is thickness of piston head, Dp is diameter of piston head, d is diameter of piston rod, h is height of gap).

Specimen	n	l	Dp	d	h	Fluid
SP-2-n1-F_2	1	5	18.8	10	0.6	ρ(p) = 2.0 g/L
SP-2-n2-F_2	2	5	18.8	10	0.6	ρ(p) = 2.0 g/L
SP-2-n3-F_2	3	5	18.8	10	0.6	ρ(p) = 2.0 g/L
SP-2-n4-F_2	4	5	18.8	10	0.6	ρ(p) = 2.0 g/L
SP-2-n1-F_3	1	5	18.8	10	0.6	ρ(p) = 3.0 g/L
SP-2-n2-F_3	2	5	18.8	10	0.6	ρ(p) = 3.0 g/L
SP-2-n3-F_3	3	5	18.8	10	0.6	ρ(p) = 3.0 g/L
SP-2-n4-F_3	4	5	18.8	10	0.6	ρ(p) = 3.0 g/L
SP-2-n1-F_4	1	5	18.8	10	0.6	ρ(p) = 4.0 g/L
SP-2-n2-F_4	2	5	18.8	10	0.6	ρ(p) = 4.0 g/L
SP-2-n3-F_4	3	5	18.8	10	0.6	ρ(p) = 4.0 g/L
SP-2-n4-F_4	4	5	18.8	10	0.6	ρ(p) = 4.0 g/L

Figure 23 shows the acceleration attenuation ratio curves for the four damper types at three-speed stages. The three specimens' attenuation ratios are significantly lower than those of the solid-state friction damper, indicating that more vibration energy is dissipated in the fluid damper and that the energy transferred to the washing machine's surface is substantially reduced. The SP-2-n3-F_2 specimen's is the smallest of the three specimens, with a reduction of 83.49% compared to the friction damper at 800 rpm.

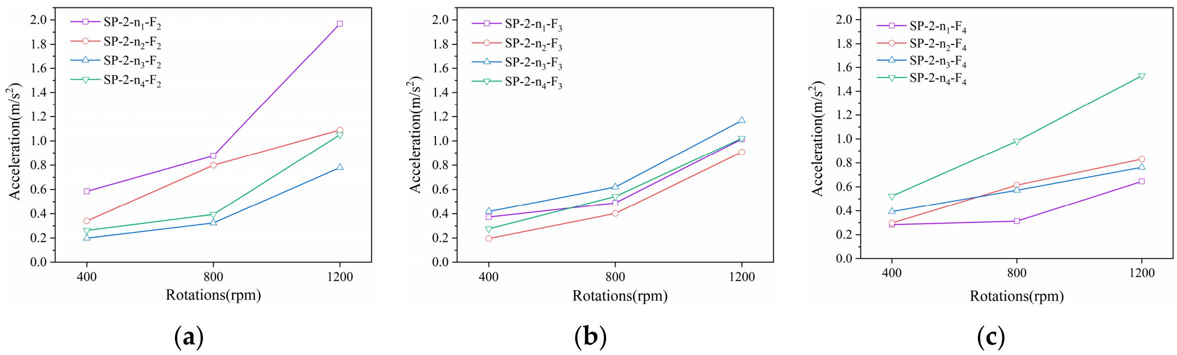

Figure 22. Average acceleration for three speed stages (bottom acceleration in z-direction, the diameter of the piston head of the specimen is 18.8 mm, changing the number of piston heads): (**a**) ρ(p) = 2.0 g/L; (**b**) ρ(p) = 3.0 g/L; (**c**) ρ(p) = 4.0 g/L.

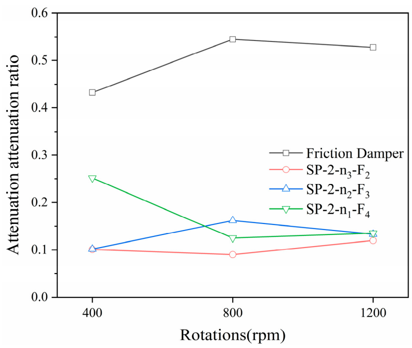

Figure 23. Acceleration attenuation ratio.

4.4. Noise Reduction

The vibration energy produced by the rotating drum passes via the spring and damper to the shell, causing the shell to vibrate and produce noise. As a result, noise and vibration are mutually synergetic [35]. During spinning, the noise rises simultaneously with the spin speed.

Concerning the noise test standards, the sound power levels of washing machine noise can be calculated according to the following equation:

$$Lw = (\overline{L}p - 2) + 10\lg\frac{S}{S0} \tag{12}$$

where, Lw is the sound power levels of the washing machine noise (dB), $\overline{L}p$ is the average sound pressure levels of the noise at the four test points (dB), S is the envelope area of the measurement surface (m^2), $S0$ is the datum area, $S0$ = 1 m^2. Let $l1$, $l2$, $l3$ are the length, width, and height of the washing machine case, respectively (dimensions in m) $a = \frac{l1}{2} + 1$, $b = \frac{l2}{2} + 1$, $c = l3 + 1$, $S = 4(ab + bc + ac)$.

Noise tests were performed on the four specimens SP-2-$n4$-F$_3$, SP-2-$n4$-F$_0$, SP-2-$n4$-F$_p$, and SP-2-$n4$-F$_w$ in Section 4.3.1, and the calculated noise sound power levels are listed in Table 8. Figure 24 illustrates the noise sound power levels Lw using these four specimens and the solid-state friction type. This indicates that a certain amount of noise reduction can be achieved with a fluid damper that uses non-Newtonian fluid as the damping fluid. When the specimen SP-2-$n4$-F$_3$ was employed in the washing machine, the noise attenuation was 6.24 dB, 7.34 dB, and 5.55 dB as opposed to the solid-state friction damper at three different speed stages above 800 rpm. Furthermore, the noise attenuation value is superior to that of specimen SP-2-$n4$-F$_p$, indicating that the created non-Newtonian fluid's rheological properties are more appropriate for this damping system and can result in a superior noise reduction effect.

Table 8. Noise sound power levels (unit: dB).

Rotations (rpm)	SP-2-n4-F_3	SP-2-n4-F_0	SP-2-n4-F_p	SP-2-n4-F_w	Friction Damper
400	57.23	63.28	61.77	62.55	60.78
800	59.14	67.49	63.87	67.35	65.38
1200	59.78	70.61	65.71	69.37	67.12
1400	62.33	73.83	66.57	69.73	67.88

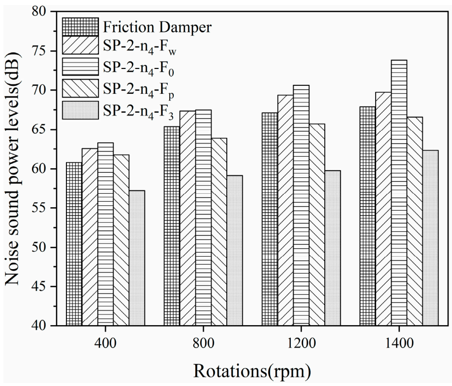

Figure 24. Noise sound power levels (friction damper and specimens SP-2-n4-F_3, SP-2-n4-F_0, SP-2-n4-F_p and SP-2-n4-F_w).

As previously mentioned in Section 4.3.4, the three specimens SP-2-n3-F_2, SP-2-n2-F_3 and SP-2-n1-F_4 show better damping effects. Figure 25 shows the noise sound power levels Lw using these three specimens and the solid-state friction type. It is evident from the comparison that the noise value using the three specimens has undergone different levels of attenuation, with a noise reduction range of 3.57–10.38 dB. Specimen SP-2-n3-F_2 achieves the most significant noise reduction effect, where the noise level was reduced by 8.85 dB, 10.14 dB, 10.38 dB, and 10.24 dB relative to the solid-state friction damper at the four-speed stages, thus demonstrating that the fluid damper can significantly reduce noise with damping vibration.

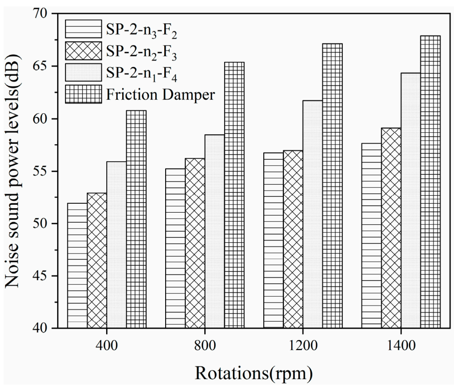

Figure 25. Noise sound power levels (friction damper and specimens SP-2-n3-F_2, SP-2-n2-F_3 and SP-2-n1-F_4).

4.5. Economical Evaluation

The non-Newtonian fluid damper designed in this study features unique originality, and the experimental results fully indicate its excellent damping performance. Moreover, its economic evaluation is indispensable for its practical application. The raw materials and manufacturing processes for the non-Newtonian fluid damper are listed in Table 9. The materials can be found with a single material type and more straightforward processing.

Compared to solid-state friction dampers, only the damping fluid and the damping head are added extra, and the damping fluid is made with food level, even industrial level powders, by heating and stirring in water. Therefore, the cost of the non-Newtonian fluid damper is similar to that of solid-state friction dampers or slightly increases, roughly estimated based on the raw materials and manufacturing process, which is a significant advantage in promotion and popularization.

Table 9. Materials and processing of main components.

Components	Raw Materials	Manufacturing Process
Connector	Plastic	Injection molding
Piston head	Plastic or Silica gel	Mold pressing
Piston rod	Metal tube	Stamping
Cylinder	Plastic	Injection molding
Sealing ring	Rubber	Mold processing
Damping fluid	Food level or industrial level powder	Dissolution

5. Conclusions

(1) Utilizing the characteristics of the pseudoplastic non-Newtonian fluid, the new gap damper made of medium-low viscosity non-Newtonian fluid with reduced stiffness compared with the traditional friction damper can effectively suppress vibration and reduce the noise of the washing machine. It can result in the attenuation of the vibration energy up to 98.44%, the reduction of the noise up to 10.38 dB, and the reduction of the acceleration attenuation ratio up to 83.49%.

(2) The theoretical formula and experimental results reveal that the output damping force can be increased by appropriately increasing the number of piston heads, increasing the diameter of the damping head, and choosing an appropriate fluid viscosity. However, it is difficult to straightforwardly obtain the best structural parameters in the real world by adjusting variables linearly.

(3) As a novel kind of fluid damper, non-Newtonian fluid would serve a more valuable and essential role owing to its intrinsic hydrodynamic characteristics. In the washing machine, the apparent elastic coefficient of the damper in the vibration-damping system should not be too rigid or too soft. The solid-state damper and the fluid damper with water or air could not effectively suppress the vibration intensity. A damper with a moderate apparent elastic coefficient could make an internal relative motion and dissipate more vibration energy.

(4) A small fluid damper was designed in accordance with the structure of a sizeable viscous fluid damper widely used in engineering to provide a satisfying damping force for washing machines. The non-Newtonian fluid damper has a simple structural design, controllable material cost, and straightforward processing conducive to popularization and application.

Author Contributions: Conceptualization, Y.S. and Z.Z.; methodology, Y.S.; software, Z.C.; data curation, Y.S.; formal analysis, X.W. and Z.Z.; writing—original draft, Y.S. and Z.Z.; writing—review and editing, X.W.; supervision, Q.F. and T.Z.; funding acquisition, T.Z.; project administration, Q.F. All authors have read and agreed to the published version of the manuscript.

Funding: This research was funded by the GuangDong Basic and Applied Basic Research Foundation (Grant No. 2022A1515011564).

Data Availability Statement: All data for this study have been included in this paper and there are no other unpublished data.

Conflicts of Interest: The authors declare no conflicts of interest.

References

1. Nygårds, T.; Berbyuk, V. Multibody modeling and vibration dynamics analysis of washing machines. *Multibody Syst. Dyn.* **2011**, *27*, 197–238. [CrossRef]
2. Cho, J.-S.; Jeong, H.-Y.; Kong, K.-C. Analysis of dynamic model of a top-loading laundry machine with a hydraulic balancer. *Int. J. Precis. Eng. Manuf.* **2014**, *15*, 1615–1623. [CrossRef]
3. Shimizu, T.; Funakoshi, H.; Kobayashi, T.; Sugimoto, K. Reduction of noise and vibration in drum type washing machine using Q-learning. *Control Eng. Pract.* **2022**, *122*, 105095. [CrossRef]
4. Kim, Y.-J.; Kim, D.-C.; Jeong, W.-B. Dynamic modeling and analysis of a quad horizontal damper system for transient vibration reduction in top loading washing machine. *J. Mech. Sci. Technol.* **2019**, *33*, 1123–1130. [CrossRef]
5. Spelta, C.; Previdi, F.; Savaresi, S.M.; Fraternale, G.; Gaudiano, N. Control of magnetorheological dampers for vibration reduction in a washing machine. *Mechatronics* **2009**, *19*, 410–421. [CrossRef]
6. Bui, Q.-D.; Nguyen, Q.H.; Hoang, L.-V.; Mai, D.-D. A new self-adaptive magneto-rheological damper for washing machines. *Smart Mater. Struct.* **2021**, *30*, 037001. [CrossRef]
7. Nguyen, Q.H.; Choi, S.B.; Woo, J.K. Optimal design of magnetorheological fluid-based dampers for front-loaded washing machines. *Proc. Inst. Mech. Eng. Part C J. Mech. Eng. Sci.* **2013**, *228*, 294–306. [CrossRef]
8. Bui, Q.-D.; Nguyen, Q.H.; Nguyen, T.T.; Mai, D.-D. Development of a Magnetorheological Damper with Self-Powered Ability for Washing Machines. *Appl. Sci.* **2020**, *10*, 4099. [CrossRef]
9. Deng, H.; Han, G.; Zhang, J.; Wang, M.; Ma, M.; Zhong, X.; Yu, L. Development of a non-piston MR suspension rod for variable mass systems. *Smart Mater. Struct.* **2018**, *27*, 065014. [CrossRef]
10. Campos, R.O.; Nicoletti, R. Vibration reduction in vertical washing machine using a rotating dynamic absorber. *J. Braz. Soc. Mech. Sci. Eng.* **2014**, *37*, 339–348. [CrossRef]
11. Liu, T.-H.; Chen, C.-G.; Lu, C.-Y. Implementation of a Sensorless Switched Reluctance Drive System for a Washing Machine with Reduced Vibration and Acoustic Noise. *Electr. Power Compon. Syst.* **2011**, *39*, 605–620. [CrossRef]
12. Buśkiewicz, J.; Pittner, G. Reduction in vibration of a washing machine by means of a disengaging damper. *Mechatronics* **2016**, *33*, 121–135. [CrossRef]
13. Jo, M.G.; Kim, J.H.; Choi, J.W. Rebalancing Method for a Front-loading Washing Machine Using a Robot Balancer System. *Int. J. Control Autom. Syst.* **2019**, *18*, 1053–1060. [CrossRef]
14. Esfandiyari, R.; Marnani, J.A.; Mousavi, S.A.; Zahrai, S.M. Seismic behavior of structural and non-structural elements in RC building with bypass viscous dampers. *Steel Compos. Struct.* **2020**, *34*, 487–497. [CrossRef]
15. Narkhede, D.I.; Sinha, R. Behavior of nonlinear fluid viscous dampers for control of shock vibrations. *J. Sound Vib.* **2014**, *333*, 80–98. [CrossRef]
16. Homik, W. Damping of torsional vibrations of ship engine crankshafts—General selection methods of viscous vibration damper. *Pol. Marit. Res.* **2011**, *18*, 43–47. [CrossRef]
17. Jia, J.; Shen, X.; Du, J.; Wang, Y.; Hua, H. Design and mechanical characteristics analysis of a new viscous damper for piping system. *Arch. Appl. Mech.* **2008**, *79*, 279–286. [CrossRef]
18. Jia, J.H.; Wu, H.W.; Hua, H.X. Test Verification of a New Type Damper for Piping System. *Adv. Mater. Res.* **2011**, *199–200*, 1046–1050. [CrossRef]
19. Hwang, J.-S.; Tseng, Y.-S. Design formulations for supplemental viscous dampers to highway bridges. *Earthq. Eng. Struct. Dyn.* **2005**, *34*, 1627–1642. [CrossRef]
20. Kono, H. Characterization and properties of carboxymethyl cellulose hydrogels crosslinked by polyethylene glycol. *Carbohydr. Polym.* **2014**, *106*, 84–93. [CrossRef]
21. Khouryieh, H.A.; Herald, T.J.; Aramouni, F.; Bean, S.; Alavi, S. Influence of deacetylation on the rheological properties of xanthan-guar interactions in dilute aqueous solutions. *J. Food Sci.* **2007**, *72*, C173–C181. [CrossRef] [PubMed]
22. Khouryieh, H.A.; Herald, T.J.; Aramouni, F.; Alavi, S. Intrinsic viscosity and viscoelastic properties of xanthan/guar mixtures in dilute solutions: Effect of salt concentration on the polymer interactions. *Food Res. Int.* **2007**, *40*, 883–893. [CrossRef]
23. Casas, J.A.; Mohedano, A.F.; Garca-Ochoa, F. Viscosity of guar gum and xanthan/guar gum mixture solutions. *J. Sci. Food Agric.* **2000**, *80*, 1722–1727. [CrossRef]
24. Liu, P.; Peng, J.; Li, J.; Wu, J. Radiation crosslinking of CMC-Na at low dose and its application as substitute for hydrogel. *Radiat. Phys. Chem.* **2005**, *72*, 635–638. [CrossRef]
25. Capanema, N.S.V.; Mansur, A.A.P.; de Jesus, A.C.; Carvalho, S.M.; de Oliveira, L.C.; Mansur, H.S. Superabsorbent crosslinked carboxymethyl cellulose-PEG hydrogels for potential wound dressing applications. *Int. J. Biol. Macromol.* **2018**, *106*, 1218–1234. [CrossRef] [PubMed]
26. Sun, C.; Boluk, Y. Rheological behavior and particle suspension capability of guar gum: Sodium tetraborate decahydrate gels containing cellulose nanofibrils. *Cellulose* **2016**, *23*, 3013–3022. [CrossRef]
27. Zhang, Z.; Pan, H.; Liu, P.; Zhao, M.; Li, X.; Zhang, Z. Boric acid incorporated on the surface of reactive nanosilica providing a nano-crosslinker with potential in guar gum fracturing fluid. *J. Appl. Polym. Sci.* **2017**, *134*, 45037. [CrossRef]
28. Li, N.; Liu, C.; Chen, W. Facile Access to Guar Gum Based Supramolecular Hydrogels with Rapid Self-Healing Ability and Multistimuli Responsive Gel-Sol Transitions. *J. Agric. Food Chem.* **2019**, *67*, 746–752. [CrossRef]

29. Saadatlou, G.A.; Pircheraghi, G. Concentrated regimes of xanthan-based hydrogels crosslinked with multifunctional crosslinkers. *Carbohydr. Polym. Technol. Appl.* **2021**, *2*, 100047. [CrossRef]
30. Simões, B.M.; Cagnin, C.; Yamashita, F.; Olivato, J.B.; Garcia, P.S.; de Oliveira, S.M.; Eiras Grossmann, M.V. Citric acid as crosslinking agent in starch/xanthan gum hydrogels produced by extrusion and thermopressing. *Lwt* **2020**, *125*, 108950. [CrossRef]
31. Jiuhong, J.; Jianye, D.; Yu, W.; Hongxing, H. Design method for fluid viscous dampers. *Arch. Appl. Mech.* **2007**, *78*, 737–746. [CrossRef]
32. Sun, J.; Jiao, S.; Huang, X.; Hua, H. Investigation into the Impact and Buffering Characteristics of a Non-Newtonian Fluid Damper: Experiment and Simulation. *Shock Vib.* **2014**, *2014*, 170464. [CrossRef]
33. McDonald, K.T. Physics in the laundromat. *Am. J. Phys.* **1998**, *66*, 209–211. [CrossRef]
34. Ding, G.; Zhou, Y.; Wu, M.; Wang, J. Improved performance of calcareous sand subgrade reinforced by soilbags under traffic load. *Proc. Inst. Civ. Eng. Geotech. Eng.* **2021**, *174*, 670–681. [CrossRef]
35. Kim, H.-G.; Nguyen, T.M.; Lee, G.; Lim, C.; Wang, S. Efficient topography optimization of a washing machine cabinet to reduce radiated noise during the dehydration process. *J. Mech. Sci. Technol.* **2021**, *35*, 973–978. [CrossRef]